PCCP

Accepted Manuscript




ROYAL SOCIETY OF CHEMISTRY

www.rsc.org/pccp

# Charge- and thickness-dependent inplane deformation of multilayer graphene thin films

Sheng Sun, Tong-Yi Zhang*

Shanghai Materials Genome Institute and Shanghai University Materials Genome Institute,

Shanghai University, Shanghai 200444, China

**Abstract:**

**The charge- and thickness-dependent inplane deformation of multilayer graphene thin films in electrolyte was studied by joint first-principles/continuum calculations (JFPCC) and the surface eigenstress model. At thermodynamic equilibrium, a multilayer graphene film exhibits initial deformation, which is asymmetric with respect to negative and positive charges and the thickness-dependent minimal inplane C-C bond length occurs at the same positive charge of about $0.0381\times10^{20}$ $|e|/m^2$ for all studied films. The surface eigenstress model was further developed to take the charge-induced deformation into account, which yields analytic formulas. The analytic formulas describe the JFPCC results well for multilayer graphene thin films with layer number larger than two and are powerful and user friendly in the understanding of the charge and thickness deformation, which will be observed in atomistic calculations and sophistical experiments on multilayer graphene thin films.**

## 1. INTRODUCTION

Electro-chemo-mechanical couplings of multilayer graphene films are becoming much attractive recently because of their promising applications in actuators [1,2], (bio-)sensors [3–5] and transistors [6,7]. In addition, multilayer graphene films can be applied as electrodes for energy storage in lithium battery and supercapacitors [8–10], in which mechanical deformation and failure due to charging/discharging cycles become an important scientific and technology issue.

* Corresponding author: zhangty@shu.edu.cn.

Comparing to extensive studies on expansion/contraction of graphite electrode induced by lithiation/delithiation [11,12], studies on purely charge-induced stress/strain in pristine graphene/graphite are few and conclusions are inconsistent yet. For graphite intercalation compounds, it was firstly reported in 1969 by X-ray diffraction that the inplane C-C bond length change contains information about charge transfer [13]. Then theoretical models [14], first-principles calculations and neutron-diffraction experiments [15] showed that the C-C bond length of graphite increased and decreased when graphite was negatively and positively charged, respectively, by charge transfer from intercalants. Recently, Rogers and Liu [16] showed further that the application of ions at two sides of graphene, mimicking double layer structures of electrolyte, can significantly increase the inplane strain. For pristine monolayer graphene, Topsakal et al. [17] showed that, by using first-principles calculations with the jellium model in which a uniform compensating charge background was applied to maintain the representative unit cell in the charge-neutral state, graphene plane expanded with positive charging, while negative charging had little effect on the plane size. They attributed the asymmetrical strain change to the artificial effect that excess electrons mostly spill out, due to the application of the plane wave basis and the periodic boundary conditions [18,19]. Also based on the jellium model but with the numerical atomic orbits basis, Verissimo-Alves et al. [20] showed that the equilibrium C-C bond length in graphene increased linearly with more electron doping, while the bond length decreased first and then increased with hole doping.

There are several electrochemical experiments that reveal length/volume change of carbon nanotube (CNT) bundles [7,21], graphene films [2,22] and nanoporous carbon materials [23] along with the charging/discharging processes. For example, more negative electrode potential (versus a saturated calomel electrode, SCE) could induce continuous stretching of CNT bundle, while a transition from shortening to stretching was observed under positive electrode potential larger than 0.7 V [21]. The dimension change transition from shrinking to expansion in graphene films was also observed when the electrode potential (vs SCE) was larger than 0.3 V [22]. In contrast, this dimension change transition was not observed in other experiments on graphene films [24,25].

When a thin film is created by cutting out from its bulk counterpart, fresh surfaces without relaxation have high surface energy. Besides, fresh surfaces are born with surface stress, called surface eigenstress [26]. Due to the high surface energy and surface eigenstress, newly created thin films have to relax. Relaxation occurs naturally and causes inplane deformation and out-plane surface eigen-displacement [27]. Charge doping can undoubtedly change the initial deformation and surface eigenstress. Knowledge on the initial deformation and surface eigenstress as a function of charge plays the central role to understand electro-chemo-mechanical couplings in multilayer graphene films, which become the work of the current letter.

In most electromechanical applications, multilayer graphene films are inside electrolytes. Previous first-principles calculations, either employing the jellium model or applying additional ions to compensate the excess charges in graphene [16,17,20], are not able to reveal the real configuration of electrode/electrolyte systems. Recently, several algorithms have been developed to couple electronic structure calculations with implicit continuum solvent models [28–34]. In these algorithms, Hartree and external potentials are calculated by modified Poisson-Boltzmann equations. This type of algorithms was placed on a solid theoretical foundation recently via the joint density functional theory (JDFT) [35], which is adopted in the present calculations. The Debye screening of ions and the dielectric response of solvent are both considered in JDFT [28].

In the present work, we show that the nonlinear behavior of inplane C-C bond length versus charge with minimal values all appear at the charge density of about $0.0381\times10^{20}$ $|e|/\mathrm{m}^2$ for graphene layers with layer number ranging from N=1 to 6. The eigenstress model of thin film[26,27,36] was further developed to describe the initial strain and surface eigenstress of graphite thin films as a function of charge and film thickness by using a power-law model for strain-charge relationship [20].

## 2. COMPUTATIONAL DETAILS

The Bernal configuration (ABAB… stacking) [37] was used in the calculated multilayer graphene. All calculations were performed by using the open-source software JDFTx[38] with the plane wave basis

and periodic boundary conditions. In all calculations, the length along the z direction (perpendicular to the graphene plane) of the primitive cell was about 40 Å and the region out of the graphene was full of electrolyte. Electrolyte was modeled with nominal dielectric constants of 78.4 (water) and ionic concentrations of 1M. For each plane in the film, two carbon atoms were included in the primitive cell with their spacing of $a$. The inplane lattice vectors had the angle of $60°$ and the length of $\sqrt{3}a$. The generalized gradient approximation (GGA) of exchange-correlation functional[39] and the ultrasoft pseudopotential with PBE scheme [40] were employed in the present work. The Monkhorst-Pack k -point meshes[41] were of $60 \times 60 \times 1$ grids and the cutoff energy was 36 Hartree ( 1 Hartree ≈ 27.2114 e V). The valence electronic configuration for C was $2s^2 2p^2$. A functional by Grimme was employed to correct the Van der Waals interactions in multilayer graphene [42]. The temperature was set to be 298 K. Electron densities, ion positions and the length of lattice vectors were all allowed to relax in all calculations. The conjugate gradient scheme[43] was used to minimize the total energy of the calculated system. The relative accuracies in the energy differences were set to be $10^{-9}$, $10^{-8}$ and $10^{-7}$ Hartree in two successive iterative steps for electron densities, ion positions and lattice length changes, respectively.

**3. RESULTS AND DISCUSSION**

Figure 1 shows the difference in plane-averaged charge density distribution along the normal direction referenced to the corresponding charge-neutral multilayer graphene films, which were calculated by fixing the nuclei of multilayer graphene films at the charge-neutral state after relaxation. Obviously, excess charges mainly locate at the outmost graphene planes and sharply decay with oscillation to zero in the interior of a multilayer graphene film. In the present work, the thickness of a multilayer graphene film is calculated to be the distance between the two outmost graphene layers plus the thickness of one single-layer graphene, because each outmost graphene layer contributes a half of the single-layer thickness to the film thickness. The thickness of a single-layer graphene is calculated based on the previous work on quantum capacitors of single-layer

graphene[44] to be 2.964 Å. The charge oscillation occurs inside a surface zone with a thickness about 0.5 nm for all multilayer graphene films, as shown in Figure 1, thereby indicating that excess charges might be treated as surface charges. Then applying Gibbs' sharp interface treatment allows one to calculate the surface charge density per unit area surface. In this circumstance, a multilayer graphene film is treated as a composite of a 3D core region, whose elastic properties are the same with the bulk counterpart of graphite, and two 2D geometric surfaces. Both 3D and 2D surfaces are assumed to be homogeneous.

The surface eigenstress model [26,27,36] was further developed here to investigate the thickness- and charge-dependent electroelastic properties of multilayer graphene films, where "surface" instead of "interface" was used between electrode and electrolyte without confusion. Figure 2 schematically illustrates the further developed surface eigenstress model. As mentioned above, a biaxial surface eigenstress $\sigma^0_{s,\ q=0}$ without any excess charge exists in the 2D fresh surfaces, when a film is created from its bulk counterpart without relaxation. Imaging that the two surfaces are separated from the core and all the 3D core and 2D surfaces are under stress-free state. At the stress-free state, each of the surfaces will show a surface eigenstrain, $\varepsilon^0_{s,q=0}$, with respect to the stress-free core. Excess charge changes the surface dimension, as shown in Figure 2, i.e., the surface charge density generates another surface eigenstrain, $\delta\varepsilon$, and surface eigenstrain with charge is given by $\varepsilon^0_{s,q} = \varepsilon^0_{s,q=0} + \delta\varepsilon$. Obviously, the surface eigenstress with excess charge $\sigma^0_{s,q}$ in the unrelaxed state is different from that without any excess charge. In the following analysis, the unrelaxed state is chosen as reference. After relaxation, the multilayer graphene film changes its inplane size and thickness. The inplane expansion/contraction is gauged by the initial strain defined by $\varepsilon^{ini}_{q=0} = \ln\left(L^{ini}_{q=0} / L_0\right)$ or $\varepsilon^{ini}_{q} = \ln\left(L^{ini}_{q} / L_0\right)$, where $L_0$ is the dimension of inplane C-C bond length in the bulk counterpart without excess charge, and $L^{ini}_{q=0}$ and $L^{ini}_{q}$ are the inplane C-C bond lengths after relaxation without and with excess charge, respectively. In the following analysis, only the subscript "*q*" is used and the case for "*q=0*" can be realized by putting the value of q=0. With

the initial strain, the surface biaxial stress is $\sigma_{s,q}^{ini} = \sigma_{s,q}^{0} + \Delta\ \sigma_{s,q}^{ini}$, where $\Delta\ \sigma_{s,q}^{ini}$ is the parallel-relaxation-induced change in the surface biaxial stress. The relaxation induces an initial strain and a biaxial stress $\sigma_{c}^{ini}$ inside the core of a multilayer film. In the surface eigenstress model, the core of a multilayer film has the same elastic properties as its bulk counterpart and is independent of excess charge. After relaxation, the total inplane force per unit length must null, i.e., $F^{ini} = F_{c}^{ini} + 2F_{s}^{ini} = 0$ with $F_{c}^{ini} = \sigma_{c}^{ini} h_{q}^{ini}$ and $F_{s}^{ini}$ being the core and surface forces per unit length, respectively. For simplicity, the relaxation induced deformation is assumed to be small and linear such that the Hooke's law can be directly applied. As indicated in the previous work [26], the linear simplification of relaxation induced deformation is sufficiently accurate for the study of surface elasticity in silicon and diamond. Thus, the change in surface stress and the core biaxial stress are expressed by $\Delta\ \sigma_{s,q}^{ini} = Y_{s,q}\varepsilon_{q}^{ini}$ and $\sigma_{c}^{ini} = Y_{c}\varepsilon_{q}^{ini}$, respectively, where $Y_{s,q}$ is the surface biaxial Young's modulus and $Y_{c}$ is the core biaxial Young's modulus. Further assuming that the surface biaxial Young's modulus is independent of excess charge, i.e., $Y_{s,q} \approx Y_{s}$, we have the force balance equation,

$$\varepsilon_{q}^{ini} Y_{c} h_{q}^{ini} + 2(\sigma_{s,q}^{0} + Y_{s}\varepsilon_{q}^{ini}) = 0. \tag{1}$$

For charge-neutral system, the surface eigenstrain $\varepsilon_{s,q=0}^{0} = -\sigma_{s,q=0}^{0}/Y_{s}$. The charge-induced surface eigenstrain is expressed by a power law, $\delta\varepsilon = -aq + b|q|^{\alpha}$, proposed by Verissimo-Alves et al.[20]. Thus the surface eigenstress is given by

$$\sigma_{s,q}^{0} = \sigma_{s,q=0}^{0} - Y_{s}\left(-aq + b|q|^{\alpha}\right). \tag{2}$$

Substituting Eq.(2) into Eq. (1) yields the initial strain with and without excess charge

$$\varepsilon_{q}^{ini} = -\frac{2\left[\sigma_{s,q=0}^{0} - Y_{s}\left(-aq + b|q|^{\alpha}\right)\right]}{Y_{c} h_{q}^{ini} + 2Y_{s}}. \tag{3}$$

The core biaxial Young's modulus $Y_{c}$ was determined from the first-principles calculations on

the bulk graphite by applying biaxial strain on the graphite plane and the traction-free condition along the directions normal to the graphite plane. The strain energy per unit volume was calculated versus applied biaxial strain and fitted by a quadratic function of $Y_c\varepsilon^2$. The determined core biaxial Young's modulus is $Y_c = 1302.69$ GPa, which is in good agree with the experimental values of Young's modulus of 1.03 TPa [45] if the Poisson ratio of 0.19 is used. The surface biaxial Young's modulus and the surface eigenstress without excess charge were determined by JDFT calculations on charge-neutral multilayer graphene films with various film thicknesses in electrode. The determined surface eigenstress without excess charge is $\sigma^0_{s,q=0} = -0.108$ N/m and surface biaxial Young's modulus is $Y_s = -258.798$ N/m. The three charge-related parameters of $a$, $b$ and $\alpha$ in Eq (3) were determined from the JDFT calculations on multilayer graphene films with various thicknesses and excess charge densities.

Figure 3(A) shows the calculated inplane initial strain versus the charge density per surface area, where the strain is referenced to inplane C-C bond length of 1.4218 Å in bulk graphite. For the charge-neutral single-layer graphene in the electrolyte, the calculated C-C bond length is about 1.4238 Å, which is consistent with the experimental value of 1.42 Å [46]. The inplane C-C bond length exhibits an asymmetrical behavior with respect to negative and positive charges. For negatively charged multilayer graphene films, the inplane C-C bond length increases monotonically with the amount of negative charge or the number of electrons, and the thicker the film is, the smaller the charge induced elongation will be. For positively charged multilayer graphene films, however, the inplane C-C bond length shortens first and then elongates, as positive charge density increases. This asymmetrical behavior has been observed in first-principles calculations on charged monolayer graphene by using the linear combination of atomic orbits and the jellium model [20]. The minimal value of the inplane C-C bond length occurs at the charge density of about $0.0381\times10^{20}$ $|e|/m^2$ ($0.2|e|$ per unit cell) for all calculated multilayer graphene films, which is slightly larger than the previously reported value of $0.06|e|$ per unit cell for monolayer graphene [20] and the difference might be attributed to different methods employed to compensate the excess charges [16,47]. The

calculation data of the initial strain versus charge density for the multilayer graphene films with the layer number ≥ 2 were fitted with Eq. (3) by the least square method and the fitting curves are also plotted in Figure 3(A), illustrating perfect fittings for graphene with layer number ≥ 3. The fitting determines the values of charge related parameters to be $a = -0.0762\times10^{-20}$ m$^2$/|e|, $b = -0.3668\times10^{-20}$ m$^{2\alpha}$/|e| and $\alpha = 1.6415 \pm 0.1097$ . The fitted value of $\alpha$ is very close to the model-predicted value of 1.5 for monolayer graphene in vacuum [20]. To clearly show the perfect agreement between the surface eigenstress model and the numerical results, the calculated initial strain is replotted in Figure 3(B) against the film thickness for the multilayer graphene films of the layer number ≥ 2 with various excess charge densities, where the theoretical predictions are also plotted by the solid curves. As expected, the thicker the film is, the better the description of the surface eigenstress model to the initial strain will be. This is because that the 2D Gibbs sharp interface approach will fail when the film thickness is too small. Nevertheless, the present work indicates that the 2D Gibbs sharp interface approach is approximately valid until the layer number of multilayer graphene films is down to three. The surface eigenstress with excess charge was calculated with Eq. (2) and the determined charge related parameters. The inset of Figure 3(A) shows the surface eigenstress versus surface charge density, where the surface eigenstress without excess charge is highlighted. With negative excess charges, the negative surface eigenstress increases its absolute value nearly linearly with the increase of the absolute negative charge density. It is the negative surface eigenstress that causes the almost linear expansion of the films. With positive excess charges, the surface eigenstress changes its sign from negative to positive at surface charge density about $0.008\times10^{20}$ $|e|$/m$^2$, and then increases its magnitude to a peak value of 0.2 N/m at surface charge density about $0.04\times10^{20}$ $|e|$/m$^2$, at which the films exhibit the largest thickness-dependent contraction. Decreasing from the peak, the surface eigenstress changes its sign again from positive to negative at surface charge density about $0.076\times10^{20}$ $|e|$/m$^2$, after that the negative surface eigenstress makes the inplane C-C length longer again.

The asymmetric behavior of the initial strain in the multiplayer graphene films with respect to negative and positive charges cannot be understood in terms of simple Coulomb repulsion between charges because it is caused by the charge redistribution inside the graphene films. As an example, Figure 4 shows the electron density distribution difference of monolayer graphene charged by $0.019\times10^{20}$ $|e|/m^2$ (0.1$|e|$ per unit cell) and $-0.019\times10^{20}$ $|e|/m^2$ (-0.1$|e|$ per unit cell) with respect to the neutral monolayer graphene. As shown in Figures 4A and 4C, in the positively charged graphene, the number of electrons locating at the two sides of graphene (the π bond) are decreasing and, at the same time, some electrons transfer to the graphene plane between the nearest C-C (the σ bond). Removing electrons from the π bond contributes to the elongation of inplane C-C bond length while adding electrons into the σ bond contributes to the shrinkage of inplane bond length. The two competitive factors result in a transition from shrinkage to elongation of inplane C-C bond length in the positively charged multilayer graphene films. When graphene is negatively charged, as shown in Figures 4B and 4D, the number of electrons on the two sides of graphene (the π* antibond) are increasing and, at the same time, electrons at the graphene plane between the nearest C-C (the σ bond) are depleting. The addition of electrons to the π* antibond and the removal of electrons from the σ bond can both lead to the C-C bond elongation. Electron transfer among the π/π* and σ bonds was also observed previously in graphite intercalation compounds by using first-principles calculations[15,48]. Figure 4(E) shows that both curves of the electron number on π/π* bond versus the excess charge and the electron number on σ bond versus excess charge are almost linear. For the multilayer graphene films, this type of charge transfer are also observed from the plane-averaged electron density distribution difference, as shown in Figure 1, where more electron transfer on the outside layers occurs than that on the inside layers.

## 4. CONCLUSIONS

The joint first-principles/continuum calculations of multilayer graphene in electrolyte revealed a monotonic expansion of inplane C-C bond length with more electrons. However, the inplane C-C

bond length shrinks first and then expands for hole doping with the transition point at about $0.0381\times10^{20}$ $|e|/m^2$. The asymmetrical charge-induced expansion/contraction can be explained by charge transfer between the $\sigma$ and $\pi/\pi^*$ bonds. The surface eigenstress model with a power-law of strain-charge relationship describes the first-principles calculation results perfectly, which predicts the charge- and thickness-dependent elastic properties of the multilayer graphene thin films. It will be straightforward to apply the developed surface eigenstress model to other types of nanomaterials such as nanowires.

**Acknowledgements:**

This work was supported by the NSFC/RGC Joint Research Fund (Project number, N_HKUST621/11) from the Hong Kong Research Grants Council, Hong Kong, China and the research grant (No.14DZ2261200) from the Science and Technology Commission of Shanghai Municipality. S. Sun also acknowledges financial support from the National Natural Science Foundation of China (No. 11202067) and the support of the high performance computing platform of Shanghai University.

**References:**

1 Y. Huang, J. Liang and Y. Chen, *J. Mater. Chem.*, 2012, **22**, 3671.

2 J. Liu, Z. Wang, X. Xie, H. Cheng, Y. Zhao and L. Qu, *J. Mater. Chem.*, 2012, **22**, 4015.

3 Y. Y. Wang, T. D. Pham, K. Zand, J. Li and P. J. Burke, *ACS Nano*, 2014, **8**, 4228–4238.

4 B. Mailly-Giacchetti, A. Hsu, H. Wang, V. Vinciguerra, F. Pappalardo, L. Occhipinti, E. Guidetti, S. Coffa, J. Kong and T. Palacios, *J. Appl. Phys.*, 2013, **114**, 084505.

5 P. K. Ang, W. Chen, A. T. S. Wee and K. P. Loh, *J. Am. Chem. Soc.*, 2008, **130**, 14392–3.

6 L. Britnell, R. V Gorbachev, A. K. Geim, L. A. Ponomarenko, A. Mishchenko, M. T. Greenaway, T. M. Fromhold, K. S. Novoselov and L. Eaves, *Nat. Commun.*, 2013, **4**, 1794.

7 B. N. Szafranek, G. Fiori, D. Schall, D. Neumaier and H. Kurz, *Nano Lett.*, 2012, **12**, 1324–8.

8 S. Bae, S. J. Kim, D. Shin, J.-H. Ahn and B. H. Hong, *Phys. Scr.*, 2012, **T146**, 014024.

9 X. Huang, Z. Zeng, Z. Fan, J. Liu and H. Zhang, *Adv. Mater.*, 2012, **24**, 5979–6004.

10 C. Xu, B. Xu, Y. Gu, Z. Xiong, X. S. Zhao and J. Sun, *Energy Environ. Sci.*, 2013, **6**, 1388.

11 D. Liu, Y. Wang, Y. Xie, L. He, J. Chen, K. Wu, R. Xu and Y. Gao, *J. Power Sources*, 2013,

**232**, 29–33.

12 A. Mukhopadhyay and B. W. Sheldon, *Prog. Mater. Sci.*, 2014, **63**, 58–116.

13 T. R. Beck, *J. Phys. Chem.*, 1969, **73**, 466–468.

14 L. Pietronero and S. Strässler, *Phys. Rev. Lett.*, 1981, **47**, 593–596.

15 C. Chan, W. Kamitakahara, K. Ho and P. Eklund, *Phys. Rev. Lett.*, 1987, **58**, 1528–1531.

16 G. W. Rogers and J. Z. Liu, *J. Am. Chem. Soc.*, 2011, **133**, 10858–63.

17 M. Topsakal and S. Ciraci, *Appl. Phys. Lett.*, 2011, **98**, 131908.

18 P. Tao, H. Guo, T. Yang and Z. Zhang, *Phys. Rev. B*, 2013, **85**, 4.

19 M. Topsakal, H. H. Gürel and S. Ciraci, *J. Phys. Chem. C*, 2013, **117**, 5943–5952.

20 M. Verissimo-Alves, B. Koiller, H. Chacham and R. Capaz, *Phys. Rev. B*, 2003, **67**, 161401.

21 R. H. Baughman, *Science*, 1999, **284**, 1340–1344.

22 J. Liang, Y. Huang, J. Oh, M. Kozlov, D. Sui, S. Fang, R. H. Baughman, Y. Ma and Y. Chen, *Adv. Funct. Mater.*, 2011, **21**, 3778–3784.

23 L. H. Shao, J. Biener, H. J. Jin, M. M. Biener, T. F. Baumann and J. Weissmüller, *Adv. Funct. Mater.*, 2012, **22**, 3029–3034.

24 X. Xie, L. Qu, C. Zhou, Y. Li, J. Zhu, H. Bai, G. Shi and L. Dai, *ACS Nano*, 2010, **4**, 6050–4.

25 X. Xie, H. Bai, G. Shi and L. Qu, *J. Mater. Chem.*, 2011, **21**, 2057.

26 T.-Y. Zhang, Z.-J. Wang and W.-K. Chan, *Phys. Rev. B*, 2010, **81**, 195427.

27 T.-Y. Zhang, H. Ren, Z.-J. Wang and S. Sun, *Acta Mater.*, 2011, **59**, 4437–4447.

28 K. Letchworth-Weaver and T. A. Arias, *Phys. Rev. B*, 2012, **86**, 075140.

29 T. Ohwaki, M. Otani, T. Ikeshoji and T. Ozaki, *J. Chem. Phys.*, 2012, **136**, 134101.

30 C. Dupont, O. Andreussi and N. Marzari, *J. Chem. Phys.*, 2013, **139**, 214110.

31 V. M. Sánchez, M. Sued and D. A. Scherlis, *J. Chem. Phys.*, 2009, **131**, 174108.

32 R. Jinnouchi and A. B. Anderson, *Phys. Rev. B*, 2008, **77**, 245417.

33 I. Hamada, O. Sugino, N. Bonnet and M. Otani, *Phys. Rev. B*, 2013, **88**, 155427.

34 J.-L. Fattebert and F. Gygi, *J. Comput. Chem.*, 2002, **23**, 662–6.

35 S. a Petrosyan, A. A. Rigos and T. A. Arias, *J. Phys. Chem. B*, 2005, **109**, 15436–44.

36 X. Zhou, H. Ren, B. Huang, T. Zhang, Z. Xiaoye, R. E. N. Hang, H. Baoling and Z. Tongyi, *Sci. China Technol. Sci.*, 2014, **57**, 680–691.

37 M. Aoki and H. Amawashi, *Solid State Commun.*, 2007, **142**, 123–127.

38 R. Sundararaman, K. Letchworth-Weaver and T. A. Arias, *{h}ttp://jdftx.sourceforge.net*, 2012.

39 J. Perdew, K. Burke and M. Ernzerhof, *Phys. Rev. Lett.*, 1996, **77**, 3865–3868.

40 D. Vanderbilt, *Phys. Rev. B*, 1990, **41**, 7892–7895.

41 H. J. Monkhorst and J. D. Pack, *Phys. Rev. B*, 1976, **13**, 5188–5192.

42 S. Grimme, *J. Comput. Chem.*, 2006, **27**, 1787–99.

43 C. Freysoldt, S. Boeck and J. Neugebauer, *Phys. Rev. B*, 2009, **79**, 241103.

44 S. Sun, Y. Qi and T.-Y. Zhang, *Electrochim. Acta*, 2015, **163**, 296–302.

45 A. Politano and G. Chiarello, *Nano Res.*, 2015, **8**, 1847–1856.

46 A. H. Castro Neto, F. Guinea, N. M. R. Peres, K. S. Novoselov and A. K. Geim, *Rev. Mod. Phys.*, 2009, **81**, 109–162.

47 L. Pastewka, P. Koskinen, C. Elsässer and M. Moseler, *Phys. Rev. B - Condens. Matter Mater. Phys.*, 2009, **80**, 1–16.

48 Y. Qi, H. Guo, L. G. Hector and A. Timmons, *J. Electrochem. Soc.*, 2010, **157**, A558.

**Figure captions**:

**Figure 1:** The difference in plane-averaged electron density distribution referenced to the corresponding charge-neutral multilayer graphene films. (A) 3 layer; (B) 4 layer; (C) 5 layer; (D) 6 layer. Balls show positions of graphene planes. Dashed vertical lines indicate film surfaces according to the definition of thickness of single-layer graphene based on quantum capacitance theory[44].

**Figure 2:** A schematic showing of the surface eigenstress/eigenstrain model to describe thickness- and charge-dependent inplane strain. (A) and (B) indicate that when graphite thin film is cut out from the bulk and its inplane size is kept fixed, there exists an intrinsic surface stress termed eigenstress ($\sigma^0_{s,\ q=0}$). (C) Charging of the film changes the surface eigenstress from $\sigma^0_{s,\ q=0}$ to $\sigma^0_{s,\ q}$ under the inplane size fixed. (D) Surface relaxation leads to initial strain. (E) and (F) illustrate the imaginary consideration of eigenstress model, in which two zero-thickness surfaces are separated from the core. The 3D core region holds all properties of the bulk counterpart while 2D surfaces induce inplane deformation and have eigenstrain $\varepsilon^0_{s,\ q}$ under eigenstress $\sigma^0_{s,\ q}$.

**Figure 3:** Initial strain versus (A) charge density per surface area and (B) film thickness (2 to 6 layers graphene). Points are calculated results and lines are predicted curves of Eq.(3). The strain is referenced to the calculated inplane C-C bond length of 1.4218 Å in bulk graphite. The inset in (A) shows the surface eigenstress as a function of charge density per surface area.

**Figure 4:** (A-D) Contour plots of electron density difference ($\Delta N$) between charged and charge-neutral single-layer graphene, where the horizontal and vertical axes are in units of angstrom and the balls indicate positions of carbon atoms and the lines between balls denote atomic bonds between nearest C-C atoms. (A) and (B) show $\Delta N$ for 0.1 |e| and -0.1 |e| per unit cell, respectively, on the plane-view of the single layer graphene, (C) and (D) show $\Delta N$ for 0.1 |e| and -0.1 |e| per unit cell, respectively, for the lateral cross-section view of the single layer graphene. (E) Total number of charges on each bond at any given excess charge per unit cell.

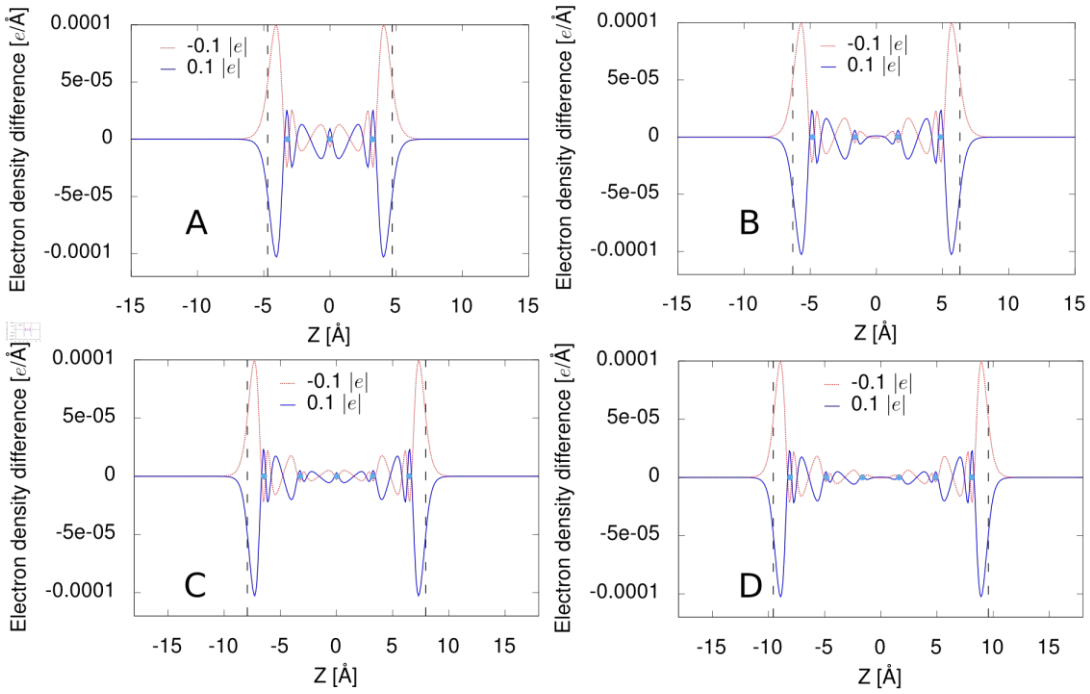


*Figure 1*

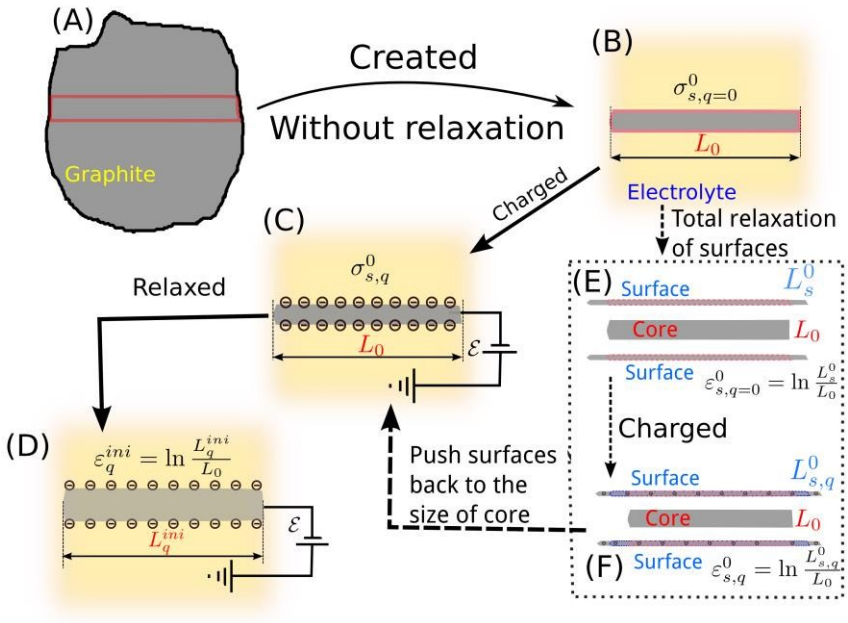


*Figure 2*

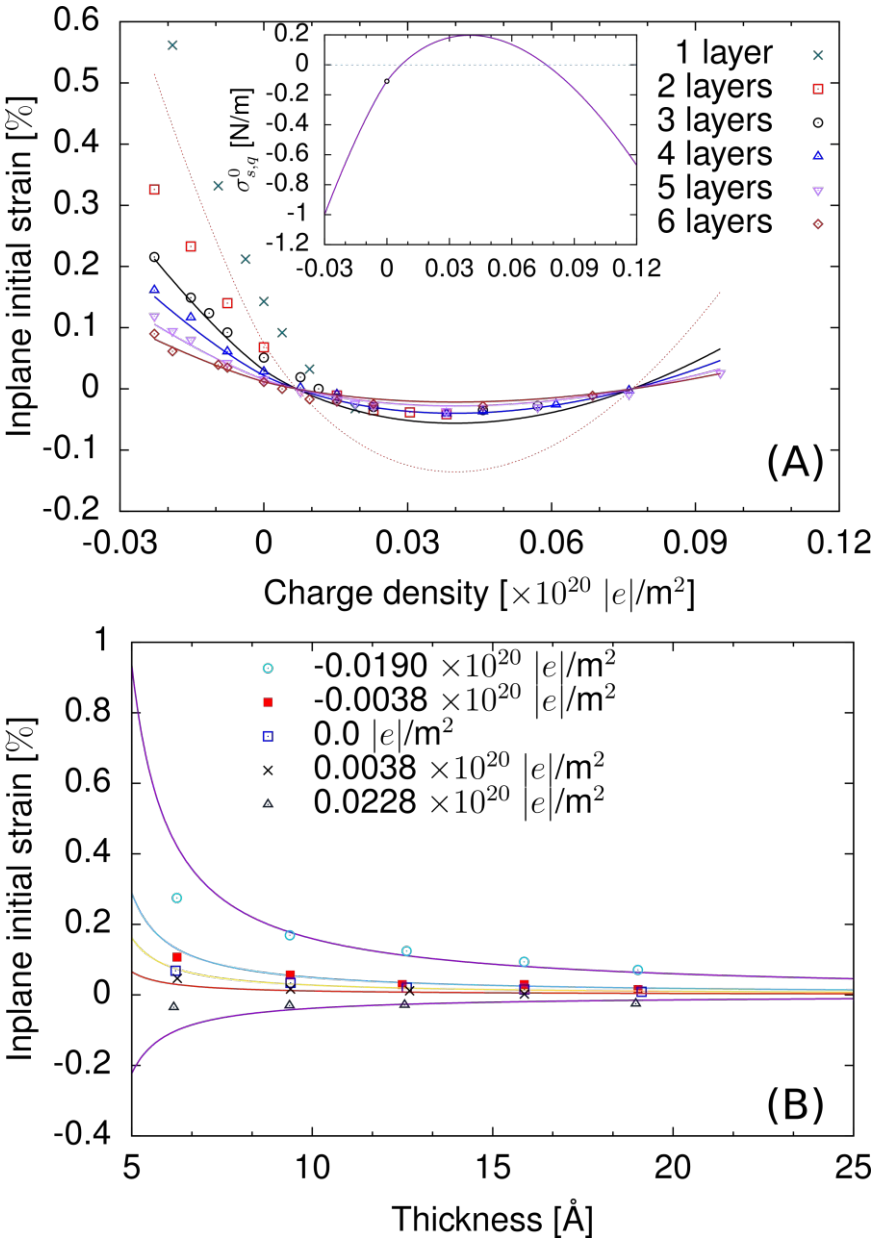


*Figure 3*

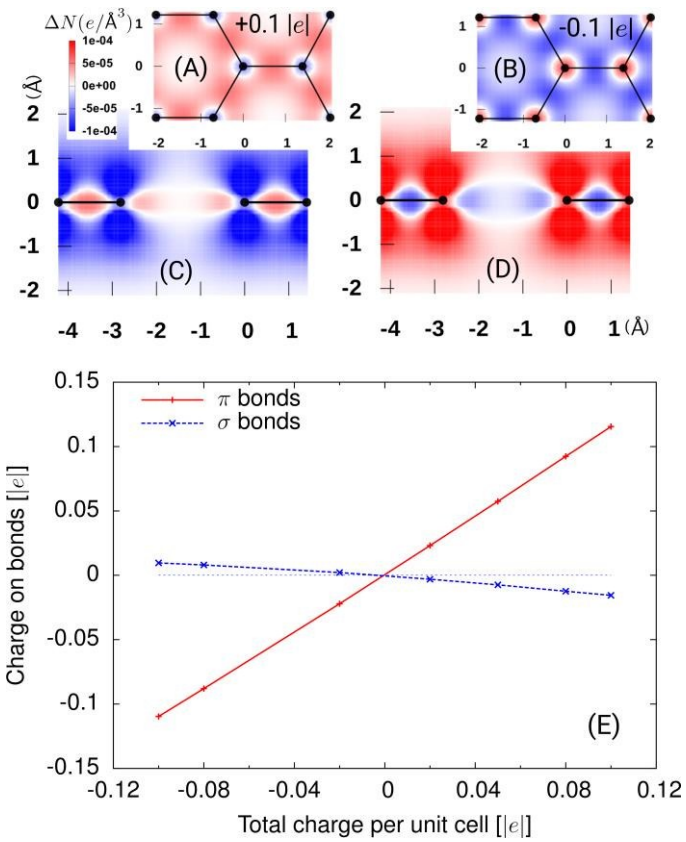


*Figure 4*